

Systematic study of transverse-momentum dependent soft function from lattice QCD

Yuan Li,¹ Shi-Cheng Xia,¹ Constantia Alexandrou,^{2,3} Krzysztof Cichy,⁴
Martha Constantinou,⁵ Xu Feng,^{1,6,7} Kyriakos Hadjiyiannakou,³ Karl Jansen,⁸
Chuan Liu,^{1,6,7} Aurora Scapellato,⁵ Fernanda Steffens,⁹ and Jacopo Tarello³

¹*School of Physics and State Key Laboratory of Nuclear Physics and Technology, Peking University, Beijing 100871, China*

²*Department of Physics, University of Cyprus, P.O. Box 20537, 1678 Nicosia, Cyprus*

³*Computation-based Science and Technology Research Center, The Cyprus Institute, 20 Kavafi Str., Nicosia 2121, Cyprus*

⁴*Faculty of Physics, Adam Mickiewicz University, ul. Uniwersytetu Poznańskiego 2, 61-614 Poznań, Poland*

⁵*Temple University, 1925 N. 12th Street, Philadelphia, PA 19122-1801, USA*

⁶*Collaborative Innovation Center of Quantum Matter, Beijing 100871, China*

⁷*Center for High Energy Physics, Peking University, Beijing 100871, China*

⁸*NIC, DESY, Platanenallee 6, D-15738 Zeuthen, Germany*

⁹*Institut für Strahlen- und Kernphysik, Rheinische Friedrich-Wilhelms-Universität Bonn, Nussallee 14-16, 53115 Bonn*

(Dated: June 25, 2021)

In this work, we perform a systematic lattice QCD study of the intrinsic, rapidity-independent soft function within the framework of large momentum effective theory. The computation is carried out using a gauge ensemble of $N_f = 2 + 1 + 1$ clover-improved twisted mass fermions. After applying an appropriate renormalization procedure and the removal of significant higher-twist contamination, we obtain the intrinsic soft function that is comparable to the one-loop perturbative result at large external momentum. The determination of the non-perturbative soft function from first principles is crucial to sharpen our understanding of the processes with small transverse momentum such as the Drell-Yan production and the semi-inclusive deep inelastic scattering. Additionally, we calculate the Collins-Soper evolution kernel using the quasi-transverse-momentum-dependent wave function as input.

Introduction – Understanding the structure of matter within the framework of Quantum Chromodynamics is one of the central goals of hadron and nuclear physics. The main physical observables used in this quest are form factors and parton distribution functions (PDFs), unified in the concept of generalized PDFs. In contrast to the collinear PDFs, which depend essentially on the fraction of the longitudinal momentum of the parent hadron carried by quarks and gluons at a given hard scale Q^2 , the transverse momentum PDFs (TMDPDF) are also dependent on the transverse momentum k_\perp carried by its constituents. Although the study of partonic transverse momentum phenomena started few years after QCD was proposed [1], our knowledge of them is limited, both experimentally and theoretically (see. e.g., [2, 3]) since, until recently, a systematic ab initio computation of TMDPDFs was out of reach.

Knowledge of TMDPDFs would open a new window in our understanding of the structure of hadrons, arising, for instance, from probing the coupling of k_\perp of a given quark with its spin [4]. However, these functions cannot be obtained from totally inclusive processes, as we need an observable in the final state carrying information on k_\perp , obtained, for example, by measuring the transverse momentum Q_\perp of a lepton pair produced in a Drell-Yan (DY) process. Consequently, they are intrinsically harder to measure. Nevertheless, the future Electron-Ion Collider in US (EIC) [5] and that in China (EicC) [6] have as one of their goals to make precise measurements of TMDPDFs, aiming to reconstruct a 3-dimensional picture of hadrons in momentum space. As in the case of

collinear PDFs, the extraction of TMDPDFs from the measured DY or semi-inclusive deep inelastic cross sections is possible, thanks to factorization theorems, which isolate the non-perturbative physics into suitable definitions of TMDPDFs [7–11]. Unfortunately, for distributions dependent on k_\perp there appears an extra divergence associated with the emission of gluons carrying small momenta, which is not canceled by the real and virtual perturbative corrections. These divergences are encoded into functions called soft functions. At large transverse momentum $Q_\perp \gg \Lambda_{\text{QCD}}$, the soft function can be calculated using perturbation theory [12, 13]. However, when the soft function captures the soft-gluon effects at small Q_\perp , it is generically non-perturbative.

Recently, using the framework of large momentum effective theory (LaMET) [14–16] a novel method has been proposed to extract the soft function from pion matrix elements [17] that can be calculated in lattice QCD, enabling a solution of the difficult problem of non-perturbatively determining the soft function. A first exploratory lattice QCD calculation was carried out by the LPC collaboration [18]. However, a better understanding of the new method with a deeper examination of the various systematic aspects involved in a lattice calculation is important in order to further establish the validity of the approach.

In this work, we perform a calculation of the soft function using a different fermion discretization scheme, namely the twisted mass fermion formulation. We demonstrate the validity of the methodology proposed by Ref. [17] and determine the soft function, showing that to

obtain the final results requires highly non-trivial steps that we develop here. These steps include the following: i) We apply an appropriate renormalization procedure to remove the power and logarithmic divergences in the non-local operator; ii) we examine various pion matrix elements and find that some of the so-called higher-twist contaminations are substantial and can even flip the sign of the matrix elements. By designing improved pion matrix elements to cancel the higher-twist effects, we show that we can reliably obtain the soft function; iii) we perform the calculation at four different pion masses in order to confirm the process-independence of the soft function; iv) we perform a detailed investigation of excited states; and v) we examine its convergence when the external momentum increases.

An important additional component of this work is the calculation of the Collins-Soper evolution kernel, where we find results that are in qualitative agreement with other lattice QCD calculations [18–20].

Theoretical framework – As proposed in Ref. [17], the intrinsic, rapidity-independent soft function $S(b_\perp, \mu)$ depends on the transverse separation b_\perp and the renormalization scale μ . Using LaMET, it can be extracted from the pion matrix element $F_\Gamma(b_\perp, P^z)$, which is defined in Euclidean spacetime as [17]

$$F_\Gamma(b_\perp, P^z) = \langle \pi(-P^z) | \bar{u}\Gamma u(b_\perp) \bar{d}\Gamma d(0) | \pi(P^z) \rangle. \quad (1)$$

Here, P^z is a large momentum in the z -direction carried by the pion. Two current operators $\bar{u}\Gamma u$ and $\bar{d}\Gamma d$ are inserted at the same timeslice, but with a spatial separation b_\perp that is perpendicular to the momentum direction. To extract the leading-twist contribution, one can choose the Dirac matrices as $\Gamma = I, \gamma_5, \gamma_\perp$ or $\gamma_5\gamma_\perp$. $F_\Gamma(b_\perp, P^z)$ can be factorized into the quasi-TMD wave function (quasi-TMDWF) Φ and the intrinsic soft function $S(b_\perp, \mu)$ [14, 17] in the large momentum limit through

$$F_\Gamma(b_\perp, P^z) \xrightarrow{P^z \rightarrow \infty} S(b_\perp, \mu) \int_0^1 dx dx' H_\Gamma(x, x', P^z, \mu) \times \Phi^\dagger(x', b_\perp, -P^z) \Phi(x, b_\perp, P^z), \quad (2)$$

where $H_\Gamma(x, x', P^z, \mu)$ is the perturbative hard kernel. The quasi-TMDWF Φ is defined as

$$\Phi(x, b_\perp, \pm P^z) = \lim_{l \rightarrow \infty} \int \frac{d\xi}{2\pi} e^{ix\xi} \phi(\pm z, b_\perp, \pm l, \pm P^z) \quad (3)$$

with $\xi = zP^z$. The wave function ϕ is given by

$$\phi(z, b_\perp, l, P^z) = \langle 0 | O_\phi(t, z, b_\perp, l) | \pi(P^z) \rangle e^{E_\pi t} \quad (4)$$

with $E_\pi = \sqrt{m_\pi^2 + P^z^2}$. The operator O_ϕ is defined as

$$O_\phi(t, z, b_\perp, l) \equiv \bar{u}(t, z/2, b_\perp) \Gamma_\phi W(z, b_\perp, l) d(t, -z/2, 0). \quad (5)$$

The quark fields \bar{u}, d and Wilson link W entering O_ϕ are all located at the same timeslice t . W has a staple shape

$(L/a)^3 \times T/a$		a (fm)		$a\mu_{sea}$		m_{sea}^π		N_{conf}	
$24^3 \times 48$		0.093		0.0053		350		126	
$a\mu_{v0}$	m_{v0}^π	$a\mu_{v1}$	m_{v1}^π	$a\mu_{v2}$	m_{v2}^π	$a\mu_{v3}$	m_{v3}^π		
0.0053	350	0.013	545	0.018	640	0.03	827		

Table I. Parameters of the ensemble used in this work. We list the spatial and temporal extents, L/a and T/a , the lattice spacing a , the sea quark mass μ_{sea} , the pion mass m_{sea}^π , the number of configurations used, N_{conf} , and four valence quark masses μ_{vi} for $i = 0, 1, 2, 3$ together with the associated pion masses m_{vi}^π . All the pion masses are given in units of MeV.

and goes through the spatial sites $(-z/2, 0) \rightarrow (-l, 0) \rightarrow (-l, b_\perp) \rightarrow (z/2, b_\perp)$. The Dirac matrix Γ_ϕ can be chosen as $\gamma_5\gamma_0$ or $\gamma_5\gamma_3$ so that Φ contains the leading-twist contribution. (Here γ_i with $i = 0, 1, 2, 3$ indicate the polarization direction t, x, y, z , respectively.)

Up to $\mathcal{O}(\alpha_s)$ corrections, the hard kernel takes a simple form, denoted here as H_Γ^0 . It can be obtained from a Fierz identity that $H_\Gamma^0 = 1/(2N_c)$ for $\Gamma = I, \gamma_\perp, \gamma_5\gamma_\perp$ and $-1/(2N_c)$ for $\Gamma = \gamma_5$ with $N_c = 3$ the number of colors. Using H_Γ^0 as an input, one can further simplify the expression (2) as

$$F_\Gamma(b_\perp, P^z) \xrightarrow[\text{LO kernel}]{P^z \rightarrow \infty} S(b_\perp, \mu) H_\Gamma^0 |\phi(z=0, b_\perp, l=\infty, P^z)|^2. \quad (6)$$

The soft function can be extracted by taking a ratio between F_Γ and $H_\Gamma^0|\phi|^2$. When using Eq. (6), one always fixes $z=0$. Thus, in the following context, the variable z is left out for simplicity.

Lattice setup – The ensemble of gauge field configurations used in this work was generated by the Extended Twisted Mass Collaboration [21]. We use the clover-improved twisted mass fermions and Iwasaki gauge action. In Eqs. (2) and (6), both F_Γ and Φ contain the structure information of the pion, which is expected to be cancelled out at sufficiently large P^z , leaving the intrinsic soft function independent of either the structure or the mass of the pion. To check such independence, we use four valence quark masses, which correspond to pion masses ranging from 827 MeV to 350 MeV. These valence quark masses together with other ensemble information are listed in Table I.

The three-point correlation function for the pion matrix element

$$C_\Gamma^{3pt}(b_\perp, P^z, t_s, t) = \frac{1}{L^3} \sum_{\vec{x}} e^{-2iP^z x_z} Z_\Gamma^2 \langle (O_\pi(t_s, -P^z) \bar{u}\Gamma u(t, \vec{x} + b_\perp) \bar{d}\Gamma d(t, \vec{x}) O_\pi^\dagger(0, P^z)) \rangle, \quad (7)$$

where t_s is the source-sink separation. The operators $\bar{u}\Gamma u$ and $\bar{d}\Gamma d$ are inserted at timeslice t and constructed using the Coulomb-gauge-fixed-wall-source operators

$$O_\pi(t, \vec{P}) = \sum_{\vec{x}, \vec{y}} \bar{u}(t, \vec{x}) \gamma_5 d(t, \vec{y}) e^{-i\vec{P}\cdot\vec{y}}, \quad (8)$$

which are known to have a good overlap with the pion ground state. Z_Γ is the renormalization factor to convert the bare lattice operator $\bar{q}\Gamma q$ to the renormalized one in the $\overline{\text{MS}}$ scheme. The pion matrix element can be obtained from the three-point function at sufficiently large t_s through

$$C_\Gamma^{3pt}\left(b_\perp, P^z, t_s, \frac{t_s}{2}\right) = \frac{|A_w(P^z)|^2}{(2E)^2} e^{-E_\pi t_s} F_\Gamma(b_\perp, P^z), \quad (9)$$

where $A_w(P^z) = L^{-\frac{3}{2}} \langle \pi(P^z) | O_\pi^\dagger(0, P^z) | 0 \rangle$ is the overlap amplitude for the pion operator. According to parity, we have $A_w(P^z) = A_w(-P^z)$.

The correlation function for the quasi-TMDWF is constructed as

$$C_{\Gamma_\phi}^{wf}(b_\perp, l, P^z, t) = \frac{Z_\phi}{L^3} \sum_{\vec{x}} e^{-iP^z x_z} \langle O_\phi(t, b_\perp, l) O_\pi^\dagger(0, P^z) \rangle, \quad (10)$$

where Z_ϕ is the renormalization factor for the staple-shaped operator, which is found to be multiplicative [22, 23]. We use $\Gamma_\phi = \gamma_5 \gamma_0$ to avoid operator mixing for Wilson-type fermions in the renormalization procedure [23]. When constructing the operator $O_\phi(t, b_\perp, l)$, we apply 5 steps of stout smearing [24] to the gauge links that enter in the Wilson line of the operator. This enables us to reduce significantly both the power divergence and the statistical noise in the correlator $C_{\Gamma_\phi}^{wf}(b_\perp, l, P^z, t)$. At large time separation t , one can extract the wave function ϕ via

$$C_{\Gamma_\phi}^{wf}(b_\perp, l, P^z, t) = \frac{A_w(P^z)}{2E} e^{-E_\pi t} \phi(b_\perp, l, P^z). \quad (11)$$

Combining Eqs. (9) and (11), the intrinsic soft function defined in Eq. (6) can be obtained through

$$S(b_\perp) = \lim_{l \rightarrow \infty} \lim_{t_s \rightarrow \infty} \frac{C_\Gamma^{3pt}\left(b_\perp, P^z, t_s, \frac{t_s}{2}\right)}{H_\Gamma^0 \left| C_{\Gamma_\phi}^{wf}\left(b_\perp, l, P^z, \frac{t_s}{2}\right) \right|^2}. \quad (12)$$

The lattice data show that $C_{\Gamma_\phi}^{wf}$ carries a small but non-vanishing imaginary part. In the determination of $S(b_\perp)$, we take into account the contributions from both the real and imaginary part of the wave function.

To examine the convergence of the lattice results at large momentum, we utilize 8 momenta with $P^z = \pm n(2\pi/L)$ for $n = 3, 4, 5, 6$, which correspond to a range from ± 1.7 GeV to ± 3.3 GeV. Given each P^z , we average the transition modes $\pi(P^z) \rightarrow \pi(-P^z)$ and $\pi(-P^z) \rightarrow \pi(P^z)$ and obtain a 15%-20% reduction in the statistical error. For each momentum, we place the wall-source operator at every two timeslices, which allows us to perform a time translation average for both C_Γ^{3pt} and $C_{\Gamma_\phi}^{wf}$. This helps to reduce the uncertainty of the soft function by nearly a factor of $\sqrt{T/2}$.

Renormalization – In our past calculation of the nucleon and Delta quasi-parton distribution functions (quasi-PDFs) [25, 26], we have utilized the

regularization-independent momentum-subtraction (RI-MOM) scheme [27] developed for non-local operators [25, 28]. The RI-MOM renormalized correlator is defined as $C_{\Gamma_\phi}^{wf,RI} = C_{\Gamma_\phi}^{wf,b} Z_\phi^{RI}$, with the renormalization factor Z_ϕ^{RI} extracted by evaluating the amputated vertex functions with quark external states. This renormalization factor cancels the power and logarithmic divergences up to some systematic effects, such as discretization effects. When using the staple-shaped operator, the systematic effects, which enter in the renormalization procedure, become more complicated. A new scheme, known as the ratio scheme [29] or the reduced ITD scheme [30], has been proposed to replace the quark-state matrix elements in RI-MOM by the corresponding hadronic ones for a better control of systematic uncertainties, such as discretization and higher-twist effects. Here, we adopt the ratio scheme and construct the renormalized correlator as

$$C_{\Gamma_\phi}^{wf,r}(b_\perp, l, P^z, t) = \frac{C_{\Gamma_\phi}^{wf,b}(b_\perp, l, P^z, t)}{C_{\Gamma_\phi}^{wf,b}(b_\perp, l, 0, t)} C_{\Gamma_\phi}^{wf,\overline{\text{MS}}}(0, 0, 0, t), \quad (13)$$

where the bare correlators $C_{\Gamma_\phi}^{wf,b}(b_\perp, l, P^z, t)$ and $C_{\Gamma_\phi}^{wf,b}(b_\perp, l, 0, t)$ contain the same operator $O_\phi(t, b_\perp, l)$ and only differ by the external momentum. Thus, one can expect that a clean cancellation of power and logarithmic divergences and other systematics can be achieved using the ratio scheme, without the introduction of an renormalization function. The coefficient $C_{\Gamma_\phi}^{wf,\overline{\text{MS}}}(0, 0, 0, t)$ is introduced to restore the correct normalization condition when $b_\perp \rightarrow 0$. As $C_{\Gamma_\phi}^{wf,\overline{\text{MS}}}(0, 0, 0, t)$ contain only local operators, it can be determined using the standard renormalization procedure as described below.

The renormalization for the local current operator $\bar{u}\Gamma u$ or $\bar{d}\Gamma d$ in C_Γ^{3pt} is straightforward. We find $Z_S^{\overline{\text{MS}}}(2 \text{ GeV}) = 0.641(3)$, $Z_P^{\overline{\text{MS}}}(2 \text{ GeV}) = 0.475(4)$ and $Z_V = 0.712(2)$, $Z_A = 0.753(3)$. Note that Z_V and Z_A are scheme- and scale-independent. These are calculated on dedicated $N_f = 4$ ensembles with the same lattice action and lattice spacing as the $N_f = 2+1+1$ ensemble used for the matrix elements. The definitions of Z_V , Z_A , Z_S and Z_P follow the convention given in Ref. [31]. Note that when the two operators $\bar{u}\Gamma u(b_\perp)$ and $\bar{d}\Gamma d(0)$ approach each other, a contact term appears and additional renormalization is required to match two bilinear quark operators to a local four-quark operator. For more details of such renormalization procedure, we refer to Refs. [32–34]. In this work, we target the soft function at $b_\perp \neq 0$ and, thus, avoid the complication of the above mentioned renormalization.

Systematic effects – In Eq. (3), the quasi-TMDWF is defined at an infinitely-large length of the Wilson line l . In a realistic lattice calculation, l is truncated by a finite lattice size. At sufficiently large l , we find that the lattice results of $|C_{\Gamma_\phi}^{wf,r}|$ converge and yield a plateau for the region of $l \gtrsim 0.8$ fm. Thus, fits to a constant lead to

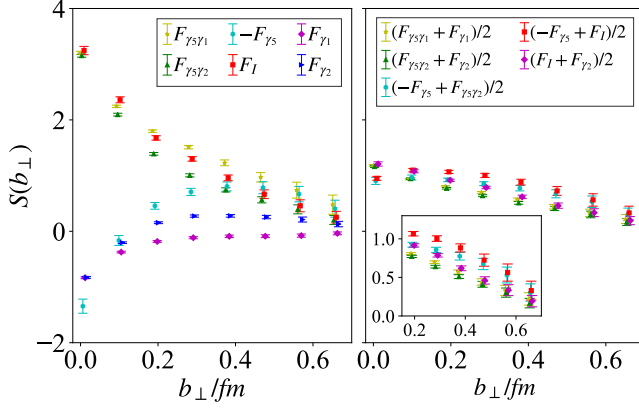


Figure 1. The intrinsic soft function $S(b_\perp)$ as a function of transverse separation b_\perp at $P^z = 6\frac{2\pi}{L} \approx 3.3$ GeV. On the left panel, $S(b_\perp)$ are compiled using the pion matrix elements F_Γ as inputs, with $\Gamma = I, \gamma_5, \gamma_\perp, \gamma_5\gamma_\perp$. For γ_\perp , there are two choices: γ_1 parallel to b_\perp and γ_2 perpendicular to b_\perp . On the right panel, $S(b_\perp)$ are compiled using the improved pion matrix elements, where the large higher-twist contamination has been cancelled significantly and the results show much better consistency.

good χ^2/dof and provide the results of $|C_{\Gamma_\phi}^{wf,r}|$ at $l \rightarrow \infty$.

To extract reliably the pion matrix element from $|C_{\Gamma_\phi}^{wf,r}|$, the excited-state contamination is another systematic effect to be controlled. Using the most precise lattice results at $P^z = 3(2\pi/L) \approx 1.7$ GeV, we find that there is a 2%-3% deviation between the soft functions obtained at $t_s/a = 8$ and 10. Therefore, we use the setup of $t_s/a = 10$ to determine the soft function at $P^z \approx 1.7$ GeV. For larger momenta, due to the rapid increase of the noise, the excited-state effects are within the reported statistical uncertainties of $t_s/a = 8$.

After taking the extrapolation of $l \rightarrow \infty$ and examining the ground-state saturation at sufficiently large t , we use the simplified notation $C_{\Gamma_\phi}^{wf}(b_\perp, P^z)$ to replace $C_{\Gamma_\phi}^{wf}(b_\perp, l, P^z, t)$ in the following context. To reveal the systematic effects more clearly, all the figures presented in this work are compiled using the most precise lattice data at $m_\pi = 827$ MeV, unless specified otherwise.

Extraction of leading-twist contribution – According to the proposal of Ref. [17], in the large momentum limit, the same intrinsic soft function can be extracted from various pion matrix elements F_Γ as far as F_Γ contain the leading-twist contribution. In this work, we make a complete investigation of the Γ dependence of the soft function. The left panel of Fig. 1 illustrates that the results of the soft function are significantly different when using various F_Γ as inputs. Some results even carry the opposite sign.

To resolve this puzzle, we check the factorization in the

LO perturbation theory and find at finite P^z

$$F_\Gamma(b_\perp, P^z) = S(b_\perp) H_\Gamma^0 |\phi(b_\perp, l, P^z)|^2 + \sum_{\Gamma' \neq \gamma_5\gamma_0, \gamma_5\gamma_3} S_{\Gamma'}(b_\perp) H_{\Gamma'}^0 |\phi_{\Gamma'}(b_\perp, l, P^z)|^2, \quad (14)$$

where the factor $H_{\Gamma'}^0$ arises from Fierz rearrangement through

$$\bar{u}\Gamma u(b_\perp)\bar{d}\Gamma d(0) = \sum_{\Gamma'} H_{\Gamma'}^0 \bar{u}(b_\perp)\Gamma' d(0)\bar{d}(0)\Gamma' u(b_\perp). \quad (15)$$

with $H_{\Gamma'}^0 = \frac{1}{16N_c} \text{Tr}(\Gamma'\Gamma\Gamma')$. The leading-twist contribution carries a factor of H_Γ^0 , which is the summation of $H_{\Gamma'}^0$, with $\Gamma' = \gamma_5\gamma_0$ and $\gamma_5\gamma_3$. The higher-twist contributions enter in the second term of Eq. (14) with the wave function $\phi_{\Gamma'}(b_\perp, l, P^z) = \langle 0|\bar{u}(b_\perp)\Gamma'W(b_\perp, l)d(0)|\pi(P^z)\rangle$. Although the higher-twist contributions are expected to be much smaller than the leading-twist one at sufficiently large momentum, in a realistic lattice calculation, where the typical size of P^z is a few GeV, the contamination from higher-twist may be significant. We find that the lattice result of $\phi_{\Gamma'}$ for $\Gamma' = \gamma_5$ is about twice larger than the leading-twist ϕ . Such large higher-twist contamination explains why some $F_\Gamma(b_\perp, P^z)$ carry the opposite sign, as observed in Fig. 1.

Note that in Fig. 1, results at the largest momentum $P^z = 6\frac{2\pi}{L} \approx 3.3$ GeV are presented. When P^z decreases, the situation becomes even worse. This is not surprising, as the leading-twist contributions are enhanced at large P^z . Considering the fact that the values of P^z accessible in the lattice calculation are quite limited, we draw the conclusion that it is essential to remove the higher-twist effects in the calculation of the soft function. Here we take two steps.

- Firstly, we calculate $\phi_{\Gamma'}$ with various Γ' and then pick up all the $\phi_{\Gamma'}$ with relatively large size. It leads to four $\phi_{\Gamma'}$ with $\Gamma' = \gamma_5, \sigma_{02}, \sigma_{12}, \sigma_{23}$. The other higher-twist $\phi_{\Gamma'}$ vanish in the LO perturbation theory and have only small sizes, as found in the lattice calculation.
- Secondly, we define improved pion matrix elements as $\sum_\Gamma c_\Gamma F_\Gamma(b_\perp, l)$, where the coefficients c_Γ (with $\Gamma = I, \gamma_5, \gamma_\perp, \gamma_5\gamma_\perp$) are chosen appropriately to cancel the contributions from $\phi_{\Gamma'}$ (with $\Gamma' = \gamma_5, \sigma_{02}, \sigma_{12}, \sigma_{23}$).

Following the above two steps, we finally obtain five improved pion matrix elements as a simple combination of two $F_\Gamma(b_\perp)$, namely

$$\begin{aligned} & \frac{1}{2}(F_{\gamma_5\gamma_1} + F_{\gamma_1}), & \frac{1}{2}(F_{\gamma_5\gamma_2} + F_{\gamma_2}), & \frac{1}{2}(-F_{\gamma_5} + F_{\gamma_5\gamma_2}), \\ & \frac{1}{2}(-F_{\gamma_5} + F_I), & \frac{1}{2}(F_I + F_{\gamma_2}). \end{aligned} \quad (16)$$

The right panel of Fig. 1 shows the soft function compiled using the five improved pion matrix elements. By

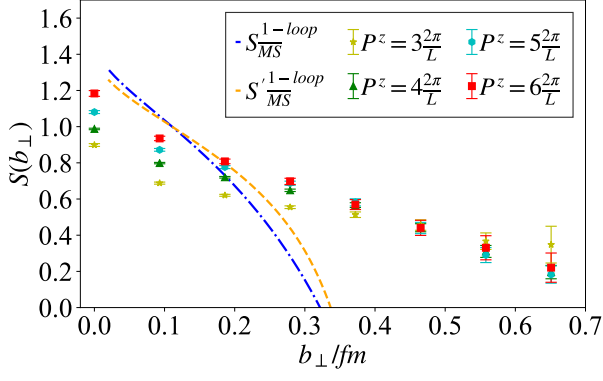


Figure 2. The lattice results of $S(b_\perp)$ for various momenta, together with the one-loop perturbative result $S_{\overline{\text{MS}}}^{1\text{-loop}}$ and its variant $S_{\overline{\text{MS}}}^{1\text{-loop}}$ with α_s including up to 4 loops. The scale μ in Eq. (17) is set as $\mu = 2$ GeV.

cancelling the dominant higher-twist effects, the results become much more consistent. The residual deviations serve as measure of important systematic effects to be controlled in future studies.

Results of the soft function – After checking the consistency among the various improved pion matrix elements, we use the choice of $\frac{1}{2}(F_{\gamma_5\gamma_1} + F_{\gamma_1})$ as an example to present the results of $S(b_\perp)$ for various momenta P^z and pion masses m_π .

In Fig. 2, $S(b_\perp, P^z)$ is shown together with the one-loop perturbative curve [35],

$$S_{\overline{\text{MS}}}(b_\perp, \mu) = 1 - \frac{\alpha_s C_F}{\pi} \ln \frac{\mu^2 b_\perp^2}{4e^{-2\gamma_E}} + \mathcal{O}(\alpha_s^2), \quad (17)$$

where one-loop and four-loop values of α_s are used at the physically most relevant scale of $S(b_\perp)$, i.e. $1/b_\perp$. The scale μ is set as $\mu = 2$ GeV. We note that the lattice results agree qualitatively with the perturbative function at around $b_\perp \sim 0.2$ fm, particularly at the largest boost and when the higher-order effects are partially included via α_s . At larger b_\perp , non-perturbative features start to set in and the decay of $S(b_\perp)$ is slower than the perturbative prediction. It is also noteworthy that the convergence of the lattice results in P^z clearly increases with b_\perp – the results from the two largest P^z are compatible for $b_\perp \gtrsim 0.2$ fm, while smaller transverse separations will need yet larger boosts to establish convergence.

In Fig. 3, we examine the pion mass dependence of the soft function. Although $S(b_\perp)$ is extracted from pion matrix elements which depend on the detailed process of $\pi(P^z) \rightarrow \pi(-P^z)$, the factorization allows us to cancel this process dependence. Performing the calculation at four pion masses, we find that the lattice results are generally consistent within statistical errors, although a small systematic increase is found when decreasing m_π . This observation supports the statement from the factorization [17] that the soft function does not depend on the

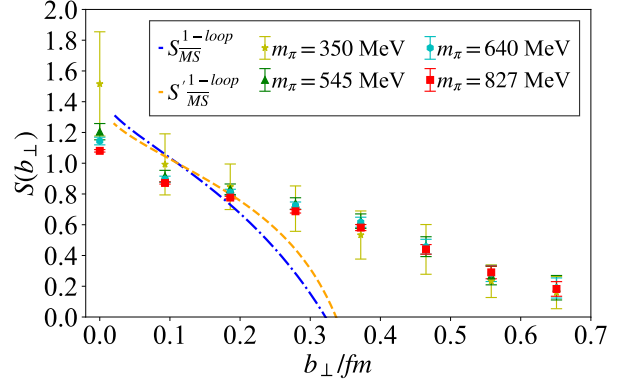


Figure 3. The intrinsic soft function $S(b_\perp)$ for the pion masses ranging from 827 MeV to 350 MeV. Here, we show results calculated at the momentum $P^z = 5 \frac{2\pi}{L}$ as an example.

detailed hadronic information from the initial/final state.

Results for the Collins-Soper kernel – The Collins-Soper kernel $K(b_\perp, \mu)$ governs the rapidity evolution of the TMDPDFs. In LaMET, the quasi-TMDPDF is factorized into the light-cone TMDPDF and a $K(b_\perp, \mu) \ln(\zeta^z/\zeta)$ factor, where $\zeta^z = 2(xP^z)^2$, with P^z playing the role of the rapidity, while ζ is the light-cone counterpart of ζ^z [36]. Thus, by taking the ratio of quasi-TMDPDFs at different values of P^z , one can extract $K(b_\perp, \mu)$. This ratio can also be expressed in terms of the quasi-TMDWFs [18] as

$$K(b_\perp, \mu) = \lim_{l \rightarrow \infty} \frac{1}{\ln(P_1^z/P_2^z)} \ln \left| \frac{\phi(b_\perp, l, P_1^z)/E_1}{\phi(b_\perp, l, P_2^z)/E_2} \right| = \frac{1}{\ln(P_1^z/P_2^z)} \ln \left| \frac{C_{\Gamma_\phi}^{wf}(b_\perp, P_1^z) C_{\Gamma_\phi}^{wf}(0, P_2^z)}{C_{\Gamma_\phi}^{wf}(b_\perp, P_2^z) C_{\Gamma_\phi}^{wf}(0, P_1^z)} \right|. \quad (18)$$

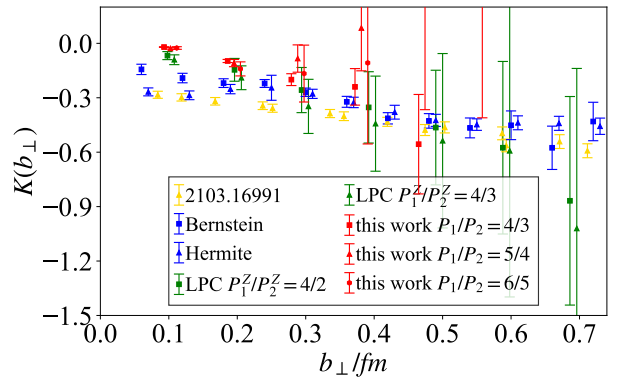


Figure 4. The lattice results for the Collins-Soper kernel $K(b_\perp, \mu)$ from various calculations, described by the color of yellow [20], blue [19], green [18] and red. The results from a same calculation are shifted horizontally to make an easier comparison.

In Fig. 4, the lattice results of $K(b_\perp, \mu)$ from this work

are shown together with data from other calculations. The results exhibit similar dependence on b_1 with some discrepancies, which indicate unquantified systematic uncertainties. Both the LPC results and ours are calculated using the quasi-TMDWFs as inputs. Thus, it is not surprising that these results are in better agreement.

Conclusion – Within the framework of the lattice formulation we calculate the intrinsic soft function introducing a number of crucial steps that enable its reliable extraction. Our work adds evidence that the methodology proposed in Ref. [17] is indeed suitable for the determination of these quantities. There is room for further improvements. For example, only the LO perturbative hard kernel is used in this calculation and future work needs to examine higher-order corrections. On the lattice side, several sources of systematics need to be addressed, including e.g. cutoff effects and further investigation of quark mass dependence towards the physical one. Nevertheless, this methodology coupled with the improvements introduced in his work, requiring synergy of perturbative and lattice QCD, is shown to be very promising and can provide important first-principle insights into transverse-momentum-dependent hadron structure.

Acknowledgement – We thank Lu-Chang Jin, Yi-Zhuang Liu, Yu-Sheng Liu, Yan-Qing Ma, Wei Wang, Yi-Bo Yang, Qi-An Zhang and Yong Zhao for valuable discussions. We thank Maximilian Schlemmer, Qi-An Zhang and Yong Zhao for providing their data of the Collins-Soper kernel. X.F. and S.C.X. are supported in part by NSFC of China under Grant No. 11775002 and National Key Research and Development Program of China under Contracts No. 2020YFA0406400. X.F. and C.L. are supported in part by NSFC of China under Grant No. 12070131001. Y.L. and C.L. are supported in part by CAS Interdisciplinary Innovation Team and NSFC of China under Grant No. 11935017. F.S. was funded by the NSFC and the Deutsche Forschungsgemeinschaft (DFG, German Research Foundation) through the funds provided to the Sino-German Collaborative Research Center TRR110 “Symmetries and the Emergence of Structure in QCD” (NSFC Grant No. 12070131001, DFG Project-ID 196253076 - TRR 110). K.C. is supported by the National Science Centre (Poland) grant SONATA BIS No. 2016/22/E/ST2/00013. K.H. is financially supported by the Cyprus Research and Innovation foundation under contract number POST-DOC/0718/0100. M.C. and A.S. acknowledge financial support by the U.S. Department of Energy, Office of Nuclear Physics, Early Career Award under Grant No. DE-SC0020405. J.T. acknowledges support from project NextQCD, co-funded by the European Regional Development Fund and the Republic of Cyprus through the Research and Innovation Foundation (EXCELLENCE/0918/0129). The calculation was carried out on TianHe-3 (prototype) at Chinese National Super-computer Center in Tianjin. This work also used compu-

tational resources from the John von Neumann-Institute for Computing on the Juwels booster system at the research center in Juelich, under the project with id ECY00 and on the Cyclone machine of the Cyprus Institute under project ID pro21a106.

-
- [1] G. Parisi and R. Petronzio, Nucl. Phys. B **154**, 427 (1979).
 - [2] I. Scimemi and A. Vladimirov, JHEP **06**, 137 (2020), 1912.06532.
 - [3] J. Collins et al., Phys. Rev. D **94**, 034014 (2016), 1605.00671.
 - [4] P. J. Mulders and R. D. Tangerman, Nucl. Phys. B **461**, 197 (1996), hep-ph/9510301, [Erratum: Nucl.Phys.B 484, 538–540 (1997)].
 - [5] R. Abdul Khalek et al., (2021), 2103.05419.
 - [6] D. P. Anderle et al., (2021), 2102.09222.
 - [7] J. C. Collins, D. E. Soper, and G. F. Sterman, Nucl. Phys. B **250**, 199 (1985).
 - [8] J. C. Collins, D. E. Soper, and G. F. Sterman, Nucl. Phys. B **308**, 833 (1988).
 - [9] X.-d. Ji, J.-p. Ma, and F. Yuan, Phys. Rev. D **71**, 034005 (2005), hep-ph/0404183.
 - [10] X.-d. Ji, J.-P. Ma, and F. Yuan, Phys. Lett. B **597**, 299 (2004), hep-ph/0405085.
 - [11] J. Collins and T. C. Rogers, Phys. Rev. D **96**, 054011 (2017), 1705.07167.
 - [12] M. G. Echevarria, I. Scimemi, and A. Vladimirov, Phys. Rev. D **93**, 054004 (2016), 1511.05590.
 - [13] Y. Li and H. X. Zhu, Phys. Rev. Lett. **118**, 022004 (2017), 1604.01404.
 - [14] X. Ji, Y.-S. Liu, Y. Liu, J.-H. Zhang, and Y. Zhao, (2020), 2004.03543.
 - [15] X. Ji, Phys. Rev. Lett. **110**, 262002 (2013), 1305.1539.
 - [16] X. Ji, Sci. China Phys. Mech. Astron. **57**, 1407 (2014), 1404.6680.
 - [17] X. Ji, Y. Liu, and Y.-S. Liu, Nucl. Phys. B **955**, 115054 (2020), 1910.11415.
 - [18] Lattice Parton, Q.-A. Zhang et al., Phys. Rev. Lett. **125**, 192001 (2020), 2005.14572.
 - [19] P. Shanahan, M. Wagman, and Y. Zhao, Phys. Rev. D **102**, 014511 (2020), 2003.06063.
 - [20] M. Schlemmer, A. Vladimirov, C. Zimmermann, M. Engelhardt, and A. Schäfer, (2021), 2103.16991.
 - [21] C. Alexandrou et al., Phys. Rev. D **98**, 054518 (2018), 1807.00495.
 - [22] M. A. Ebert, I. W. Stewart, and Y. Zhao, JHEP **03**, 099 (2020), 1910.08569.
 - [23] M. Constantinou, H. Panagopoulos, and G. Spanoudes, Phys. Rev. D **99**, 074508 (2019), 1901.03862.
 - [24] C. Morningstar and M. J. Peardon, Phys. Rev. D **69**, 054501 (2004), hep-lat/0311018.
 - [25] C. Alexandrou et al., Nucl. Phys. B **923**, 394 (2017), 1706.00265.
 - [26] Y. Chai et al., Phys. Rev. D **102**, 014508 (2020), 2002.12044.
 - [27] G. Martinelli, C. Pittori, C. T. Sachrajda, M. Testa, and A. Vladikas, Nucl. Phys. B **445**, 81 (1995), hep-lat/9411010.
 - [28] M. Constantinou and H. Panagopoulos, Phys. Rev. D

- 96**, 054506 (2017), 1705.11193.
- [29] X. Gao *et al.*, Phys. Rev. D **102**, 094513 (2020), 2007.06590.
 - [30] K. Orginos, A. Radyushkin, J. Karpie, and S. Zafeiropoulos, Phys. Rev. D **96**, 094503 (2017), 1706.05373.
 - [31] ETM, C. Alexandrou, M. Constantinou, and H. Panagopoulos, Phys. Rev. D **95**, 034505 (2017), 1509.00213.
 - [32] RBC, UKQCD, N. H. Christ, X. Feng, A. Portelli, and C. T. Sachrajda, Phys. Rev. D **93**, 114517 (2016), 1605.04442.
 - [33] Z. Bai *et al.*, Phys. Rev. Lett. **118**, 252001 (2017), 1701.02858.
 - [34] Z. Bai *et al.*, Phys. Rev. D **98**, 074509 (2018), 1806.11520.
 - [35] X. Ji, J. ping Ma, and F. Yuan, (2004), arXiv:hep-ph/0404183.
 - [36] M. A. Ebert, I. W. Stewart, and Y. Zhao, Phys. Rev. D **99**, 034505 (2019), 1811.00026.

SUPPLEMENTARY MATERIAL

In this section, we expand on a selection of technical details and add results to facilitate cross-checks of different calculations of the soft function.

Extrapolation of $l \rightarrow \infty$ – Although in the lattice QCD calculation the length of the Wilson link l is not allowed to be larger than half of the lattice size $L/2$, it is straightforward to explore the limit of $l \rightarrow \infty$ if the renormalized correlation function $|C_{\Gamma_\phi}^{wf,r}|$ has a plateau at large l . In Fig. 5, we show two examples with the external momentum $P^z = 3\frac{2\pi}{L}$ and $5\frac{2\pi}{L}$. In both cases, the plateau appears when $l \geq 0.84$ fm. Using a correlated fit to the constant and extrapolating to the $l \rightarrow \infty$ limit, we finally obtain the results of $|C_{\Gamma_\phi}^{wf,r}|$ at $l = \infty$.

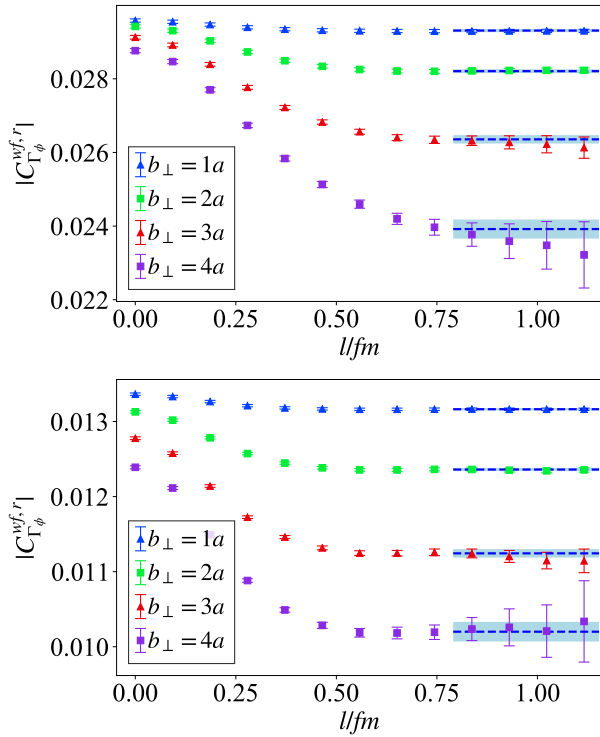


Figure 5. The l dependence of the renormalized correlation function $|C_{\Gamma_\phi}^{wf,r}|$ at $P^z = 3\frac{2\pi}{L}$ (top) and $5\frac{2\pi}{L}$ (bottom). Results at four different b_\perp are shown. The χ^2/dof , which describes the quality of the correlated fit, is listed as $\{1.1, 0.3, 0.4, 0.6\}$ for the case of $P^z = 3\frac{2\pi}{L}$ and $\{0.8, 1.4, 0.4, 0.3\}$ for $5\frac{2\pi}{L}$.

Examination of the excited-state effects – We examined the excited-state contamination of the soft function for various momenta P^z . Here, we show the case of $P^z = 3\frac{2\pi}{L}$ and $5\frac{2\pi}{L}$ as an example. In Fig. 6, we compare the soft function at the source-sink separation $t_s/a = 8$ and 10. At the smallest momentum $P^z = 3\frac{2\pi}{L}$, where the lattice results are most precise, the comparison shows about 2%-3% deviation for $S(b_\perp)$ at $b_\perp/a = 0, 1, 2, 3$. These deviations are small compared to other systematic

effects. To be conservative, we use $t_s/a = 10$ to determine the $S(b_\perp)$ at $P^z = 3\frac{2\pi}{L}$. When P^z increases, the statistical uncertainties increase significantly. At $P^z = 5\frac{2\pi}{L}$, the results of $S(b_\perp)$ are fully consistent between the cases of $t_s/a = 8$ and 10. By using $t_s/a = 10$ for $P^z = 3\frac{2\pi}{L}$ and $t_s/a = 8$ for the other momenta, we expect that the excited-state effects are under control in our analysis.

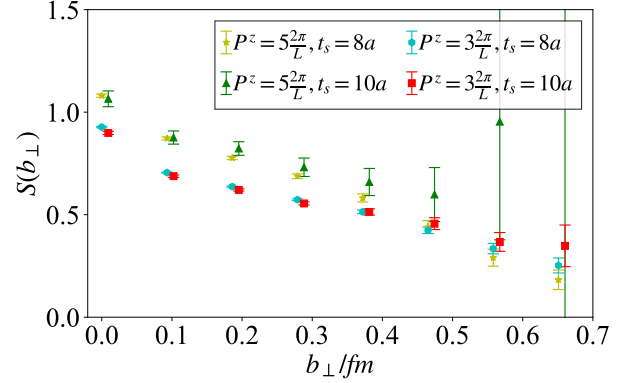


Figure 6. A comparison is made for the soft function $S(b_\perp)$ determined using the source-sink separation $t_s/a = 8$ and 10. At momentum $P^z = 3\frac{2\pi}{L}$, 2%-3% deviations are found at $b_\perp/a = 0, 1, 2, 3$. For the larger momentum $P^z = 5\frac{2\pi}{L}$, the results for $t_s/a = 8$ and 10 are all consistent.

Removal of the higher-twist contamination – In Fig. 7, we show the bare correlators $|C_{\Gamma'}^{wf}(b_\perp, l, P^z, t)|$ as a function of b_\perp for various Γ' . Only the correlation functions $|C_{\gamma_5\gamma_0}^{wf}|$ and $|C_{\gamma_5\gamma_3}^{wf}|$ contain the leading-twist contribution, while all the others also contain a higher-twist contribution. We obtain from the figure that some higher-twist correlators have comparable size to the leading-twist ones. We, thus, identify the four largest higher-twist correlators with $\Gamma' = \gamma_5, \sigma_{02}, \sigma_{12}, \sigma_{23}$. The next step to remove the large higher-twist effects is to form appropriate combinations of F_Γ with $\Gamma = I, \gamma_5, \gamma_\perp, \gamma_5\gamma_\perp$.

$\Gamma' \setminus \Gamma$	I	γ_1	γ_2	γ_5	$\gamma_5\gamma_1$	$\gamma_5\gamma_2$
$\gamma_5\gamma_0$	1/4	1/4	1/4	-1/4	1/4	1/4
$\gamma_5\gamma_3$	1/4	1/4	1/4	-1/4	1/4	1/4
γ_5	-1/4	1/4	1/4	-1/4	-1/4	-1/4
σ_{02}	-1/4	-1/4	1/4	-1/4	1/4	-1/4
σ_{12}	-1/4	1/4	1/4	-1/4	-1/4	-1/4
σ_{23}	-1/4	-1/4	1/4	-1/4	1/4	-1/4

Table SI. Leading-order hard kernel $H_{\Gamma'}^0$, using the Euclidean gamma matrices as input. All values from the table should be multiplied by a factor of $1/N_c$.

In Table SI, the values of the LO hard kernel $H_{\Gamma'}^0 = \frac{1}{16N_c} \text{Tr}(\Gamma'\Gamma')$ are shown for $\Gamma = I, \gamma_5, \gamma_\perp, \gamma_5\gamma_\perp$ associated with $\Gamma' = \gamma_5\gamma_0, \gamma_5\gamma_3$ (leading twist) and $\Gamma' =$

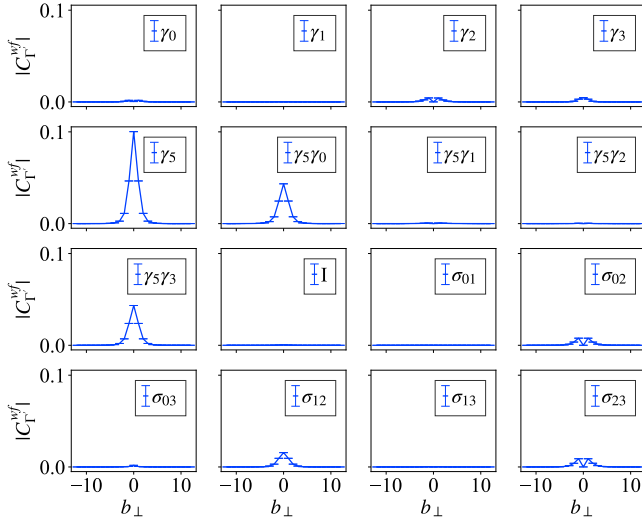


Figure 7. The bare correlators $|C_{\Gamma'}^{wf}(b_{\perp}, l, P^z, t)|$ as a function of b_{\perp} for various Γ' .

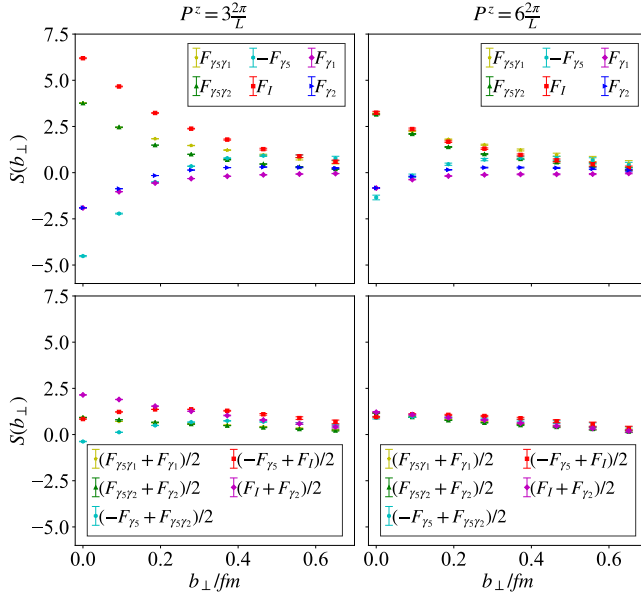


Figure 8. Examination of the convergence of the soft function when P^z increases.

$\gamma_5, \sigma_{02}, \sigma_{12}, \sigma_{23}$ (higher twist). Using the information from Table SI, we construct the five improved pion matrix elements given in Eq. (16).

In Fig. 8, we examine the convergence of the soft function when P^z increases. For a comparison, we show the results using the F_{Γ} with $\Gamma = I, \gamma_5, \gamma_1, \gamma_5\gamma_1$ in the upper panel and the results using the improved pion matrix elements in the lower panel. From left to right, the momentum P^z increases from $3\frac{2\pi}{L}$ to $6\frac{2\pi}{L}$ and better convergence is observed at larger momentum. Unfortunately, due to the large higher-twist contamination, even at $P^z = 6\frac{2\pi}{L}$ F_{Γ} with various Γ still show a strong variation. On the other hand, the improved pion matrix elements show much better convergence, demonstrating that the higher-twist effects are reduced significantly.